Dual-Band (28,38) GHz Coupled Quarter-Mode Substrate-Integrated Waveguide Antenna Array for Next-Generation Wireless Systems

Thomas Deckmyn, *Student Member, IEEE*, Maarten Cauwe, *Member, IEEE*,
Dries Vande Ginste, *Senior Member, IEEE*, Hendrik Rogier, *Senior Member, IEEE*,
and Sam Agneessens, *Member, IEEE*

Abstract— A novel dual-band substrate-integrated waveguide (SIW) antenna array topology is proposed for operation in the 28 and 38 GHz frequency bands. Four miniaturized quarter-mode SIW cavities are tightly coupled, causing mode bifurcation, and yielding an antenna topology with four distinct resonance frequencies. A pair of resonances is assigned to both the 28 and 38 GHz band, achieving wideband operation in both frequency ranges. Moreover, owing to the exploited miniaturization technique, an extremely compact array topology is obtained, facilitating easy and straightforward integration. The computer-aided design process yields a four-element antenna array that entirely covers the 28 GHz band (27.5–29.5 GHz) and 38 GHz band (37.0–38.6 GHz) with a measured impedance bandwidth of 3.65 and 2.19 GHz, respectively. A measured broadside gain of 10.1 dBi, a radiation efficiency of 75.75% and a 3 dB beamwidth of 25° are achieved in the 28 GHz band. Moreover, in the 38 GHz band, the measured broadside gain amounts to 10.2 dBi, a radiation efficiency of 70.65% is achieved, and the 3 dB beamwidth is 20°.

Index Terms— 28 GHz, 38 GHz, antenna array, coupled resonators, dual band, quarter-mode substrate-integrated waveguide (QMSIW), SIW antenna.

I. INTRODUCTION

MEETING the evermore stringent requirements for next-generation wireless systems inevitably requires a shift toward millimeter-wave (mm-Wave) operating frequencies. Novel applications, of which 5G mobile communication is a prime example, are in need for extremely high data rates. Bandwidths of several gigahertz are a necessity and, hence,

the main motivation for the shift toward the available spectrum at mm-Wave frequencies.

The mm-Wave spectrum around 28 GHz (27.5–29.5 GHz) and 38 GHz (37–38.6 GHz) is under strong consideration for next-generation 5G wireless systems, which would allow a significant performance improvement with respect to fourth-generation networks. For 5G communication, multiband antennas form an attractive solution, since multiple frequency ranges of interest can be covered by one single radiating element. This is even more so for the spectrum in the (28,38) GHz band, if it should be allocated for frequency-division duplexing. Nevertheless, antenna arrays will be a necessity to overcome the heavily increased path loss at these high-operating frequencies.

Another trend is the extensive miniaturization of electronic devices, and specifically antennas, to facilitate easy integration into 5G user equipment. Nevertheless, antenna miniaturization techniques often have unfavorable implications on the functionality of the device. Compact antenna footprints are desirable but not at the expense of crucial and indispensable antenna performance. Clearly, there is a need for novel miniaturized, low-cost 5G antenna topologies that exhibit excellent functionality in terms of bandwidth, gain, and efficiency.

The very promising substrate-integrated waveguide (SIW) technology [1] is gaining a lot of interest in the mm-Wave research field. This can be attributed to its excellent isolation and low loss, comparable to solid-metal rectangular waveguides while maintaining compatibility with standard printed circuit board (PCB) manufacturing. Moreover, its excellent shielding properties, due to the confinement of the electromagnetic fields within the SIW structure, allow for close-proximity integration of active electronics [2]–[6]. A rectangular SIW cavity can be miniaturized by bisecting it twice along two virtual quasi-magnetic walls, yielding quarter-mode SIW (QMSIW) cavities. This technique preserves the field distribution of the original SIW cavity and yields miniaturized cavities with excellent microwave performance [7], [8].

In this paper, a novel SIW dual-band antenna topology is proposed for operation in the 28 and 38 GHz bands, presently considered for 5G wireless applications. An innovative approach, based on four miniaturized coupled

QMSIW resonating cavities, is exploited to achieve stable and wideband performance in both targeted frequency bands. Wideband behavior is achieved by means of mode bifurcation, owing to the strong coupling between the QMSIW resonators. In [9], the principle of mode bifurcation through coupling of three miniaturized SIW cavities was applied to obtain wideband performance in the 60 GHz band. Nevertheless, the work proposed in this paper further improves this technique for dual-band operation, and, consequently, significantly broadens frequency ranges, necessitating an intricate optimization of the coupling between four adjacent cavities and novel wideband feeding techniques.

The four antenna cavities are skillfully combined into a footprint on the order of a conventional half-wavelength SIW antenna, resulting in an extremely compact antenna design, while obtaining excellent dual-band performance. The large bandwidth facilitates high data rates in both bands, while the small footprint enables easy integration in 5G user equipment.

Furthermore, in this paper, four such antenna elements, each consisting of four cavities, are combined into a small 1×4 antenna array, which is manufactured and fully characterized, validating its excellent radiation characteristics in both bands. Such a linear array can typically be deployed in, e.g., 5G base station equipment.

Up until now, the majority of the dual-band antenna topologies proposed in the literature relies on resonant slots. SIW slot arrays [10] achieve multiband performance in a straightforward manner but suffer from narrowband characteristics and bulky footprints, as every additional band requires a separate antenna element with a footprint in the order of half a wavelength. Ring slot [11], [12] or resonant slot [13], [14] antennas exhibit bandwidth-limited behavior and low antenna/platform isolation, making close integration with active electronics virtually impossible. Conversely, cavity-backed slot antennas [15]–[18] exhibit excellent electromagnetic shielding capabilities but generally rely on resonant slots, limiting the bandwidth. Dual-band antennas based on higher order modes [19], [20] exhibit a predetermined frequency spacing between different bands of operation. Very often, the resonance frequencies are not independently tunable, yielding less versatile performance. In [21], several cavity-backed slot antennas with distinct resonance frequencies are coupled through inductive windows, yielding multiband operation. This approach causes the antenna dimensions to increase exponentially. Moreover, it prohibits the construction of an antenna array, which is a significant drawback at mm-Wave frequencies.

This paper is organized as follows. In Section II, the novel dual-band SIW topology is proposed and its principle of operation is discussed. In Section III, the performance of the constructed antenna array is discussed, while Section IV focusses on the applied manufacturing technologies and techniques. The performance of the manufactured prototype is validated in Section V. Conclusions are presented in Section VI.

II. ANTENNA PRINCIPLE OF OPERATION

A. Dual-Band Operation Through Coupled Cavities

The proposed dual-band SIW antenna topology is depicted in Fig. 1, with its dimensions summarized in Table I.
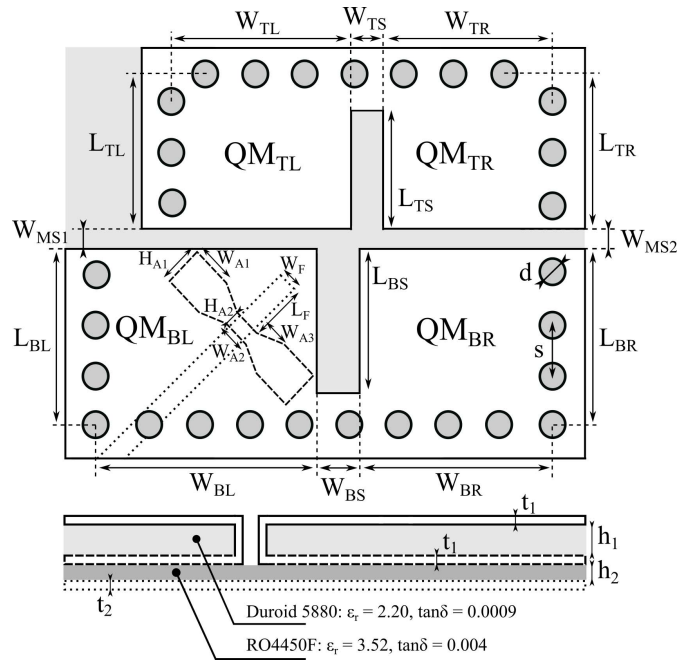

Fig. 1. Proposed dual-band SIW antenna topology, consisting of four coupled quarter-mode (QMSIW) resonant cavities, and corresponding PCB stack-up. The antenna is fed by means of aperture coupling, with an hourglass-shaped slot for maximum matching bandwidth. (Geometrical dimensions: see Table I.)

TABLE I
DIMENSIONS FOR THE NOVEL DUAL-BAND
COUPLED QMSIW ANTENNA TOPOLOGY

						Dimensions (mm)
W_{TL}	1.85	W_{BL}	2.43	W_F	0.20	
L_{TL}	1.65	L_{BL}	2.00	L_F	0.48	
W_{TR}	2.03	W_{BR}	2.40	W_{A1}	0.50	
L_{TR}	1.65	L_{BR}	2.00	H_{A1}	0.69	
W_{TS}	0.60	W_{BS}	0.48	W_{A2}	0.25	
L_{TS}	1.35	L_{BS}	1.71	H_{A2}	0.28	
W_{MS1}	0.11	W_{MS2}	0.14	W_{A3}	0.70	
s	0.40	d	0.25	h_1	0.508	
h_2	0.10	t_1	0.035	t_2	0.018	

It consists of four coupled QMSIW resonant cavities. The four coupled cavities are combined into an extremely compact topology with a footprint comparable to conventional half-wavelength planar antennas. The bottom two QMSIW resonators (QM_{BL} and QM_{BR}) are strongly coupled, effectively causing mode bifurcation. As such, two distinct cavity resonances are obtained. These are carefully distributed over the frequency range of interest, yielding wideband performance. Here, the cavity resonances in QM_{BL} and QM_{BR} cover the lower 5G band, being 27.5–29.5 GHz. The same reasoning holds for QM_{TL} and QM_{TR}, which cover the highest 5G band from 37 to 38.6 GHz.

As shown in Fig. 1, only one QMSIW cavity, i.e., QM_{BL}, is fed by microstrip aperture coupling. The remaining parasitic resonators are excited through strong proximity coupling with the feeding cavity QM_{BL}. An hourglass-shaped aperture is used to maximize the matching bandwidth. Exploiting aperture
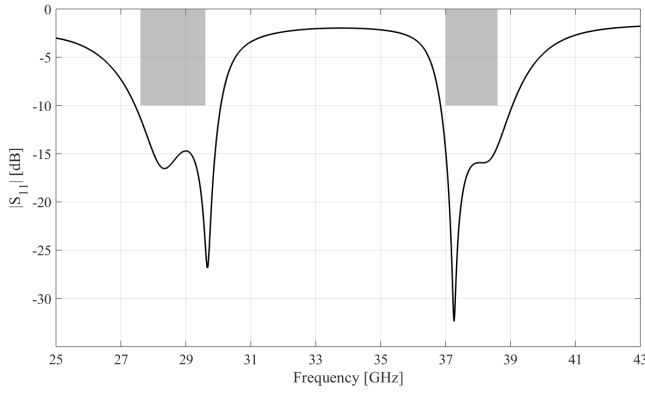
Fig. 2. Simulated reflection coefficient: two 5G bands are covered: 27.5–29.5 and 37–38.6 GHz. Two distinct resonances are observed in both frequency bands.

coupling also provides shielding between the antenna and the feeding network, significantly reducing parasitic radiation, and benefiting the radiation pattern purity. The amount of back radiation is minimized by realizing the feeding network on a thin bottom substrate layer.

Fig. 2 depicts the simulated magnitude of the reflection coefficient $|S_{11}|$. In both the 28 GHz band and 38 GHz band, two distinct resonance peaks are visible owing to mode bifurcation caused by the strongly coupled cavities QM_{BL} and QM_{BR}, and QM_{TL} and QM_{TR}, respectively. A -10 dB impedance bandwidth of 2.6 GHz in the 28 GHz band and 2.2 GHz in the 38 GHz band is achieved, completely covering the two 5G frequency bands from 27.5 to 29.5 GHz and from 37.0 to 38.6 GHz.

The simulated electric field distribution inside the resonant cavities is shown in Fig. 3, for both the 28 and 38 GHz bands. It is clear that the electric field is dominant in QM_{BL} and QM_{BR} at 29.7 GHz and, conversely, dominant in QM_{TL} and QM_{TR} at 38.3 GHz. This validates the principle of operation discussed earlier and confirms that the bottom two QMSIWs resonate in the lowest 5G band, and the top two cavities operate in the highest band.

An additional benefit of exploiting SIW technology is its excellent electromagnetic shielding capabilities, yielding high antenna/platform isolation. Not only does this allow for integration of active electronics in close proximity of the antenna but also facilitates extremely compact antenna arrays, as mutual coupling between adjacent array elements is minimal.

B. Analysis of Antenna Parameters

Fig. 4 depicts the simulated reflection coefficient for variations on the lengths L_{TL} and L_{TR} of the resonating cavities QM_{TL} and QM_{TR}, respectively. Obviously, increasing the lengths of both QMSIWs causes the pair of resonances in the 38 GHz band to shift to lower frequencies. Alternatively, when the lengths are decreased, the resonances shift to higher frequencies. In the process, the pair of resonances in the 28 GHz band remains unaffected. Hence, independent tuning in both frequency bands is possible. Similar results are obtained for the parameter pair L_{BL} and L_{BR}.
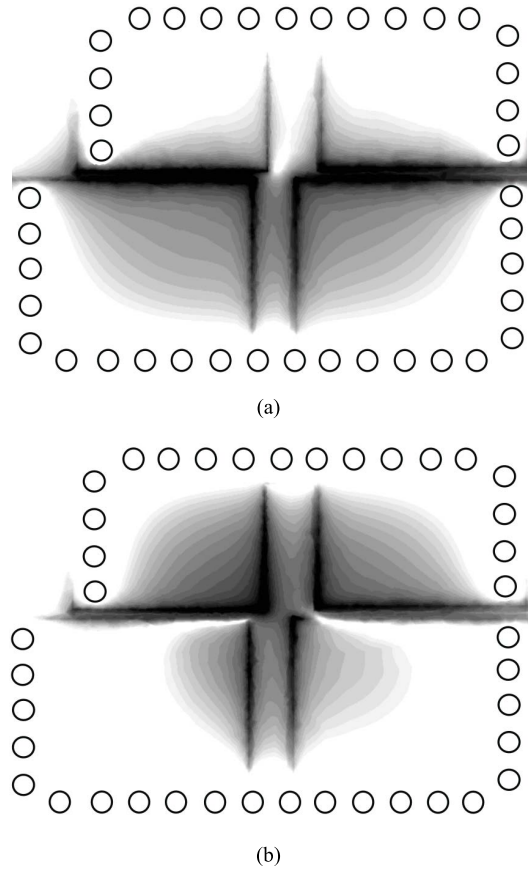

(a)

(b)

Fig. 3. Simulated normalized electric field distribution observed inside the resonant cavities. (a) At the second resonance in the lowest 5G band (field dominant in bottom two-coupled cavities QM_{BL} and QM_{BR}). (b) At the second resonance in the highest band (field dominant in top two-coupled cavities QM_{TL} and QM_{TR}).
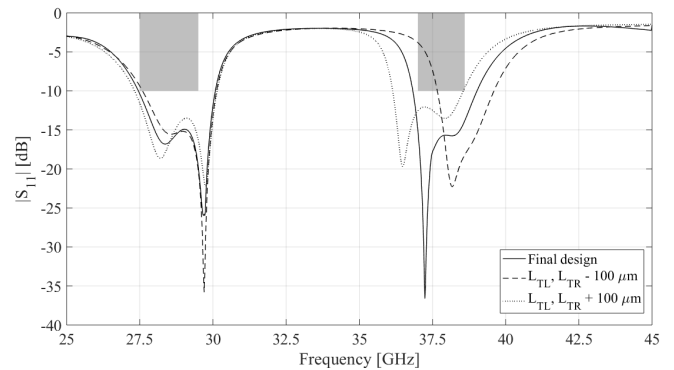

Fig. 4. Simulated reflection coefficient for variations on the cavity lengths L_{TL} and L_{TR}. Final design (full line), L_{TL}, $L_{TR} - 100$ μm (dashed line), and L_{TL}, $L_{TR} + 100$ μm (dotted line).

Fig. 5 shows the simulated reflection coefficient for variations on the slot width W_{BS}. This slot determines the amount of coupling between the QMSIW cavities that resonate in the 28 GHz band. As is apparent from Fig. 5, when the slot width W_{BS} is decreased, the amount of coupling between the adjacent resonating cavities QM_{BL} and QM_{BR} increases and, consequently, the two resonances diverge [22]. Similarly, when the slot width is increased, the coupling decreases and the resonances merge. This reasoning also holds for the QMSIWs
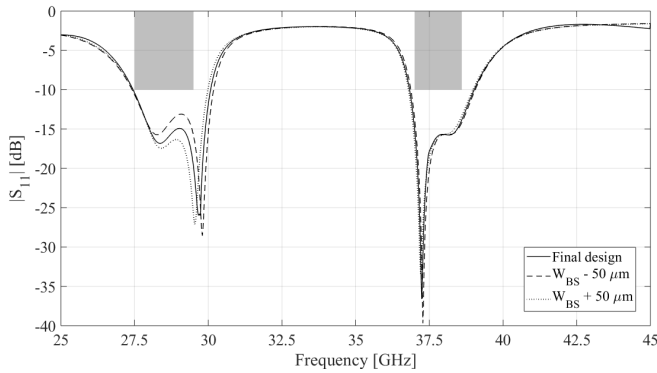
Fig. 5. Simulated reflection coefficient for variations on the slot width W_{BS}. Final design (full line), $W_{BS} - 50$ μm (dashed line), and $W_{BS} + 50$ μm (dotted line).
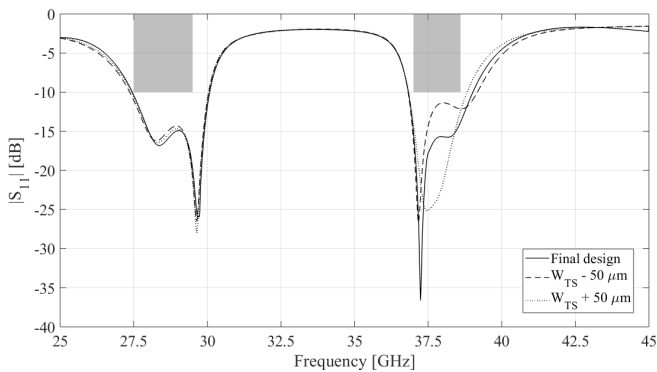

Fig. 6. Simulated reflection coefficient for variations on the slot width W_{TS}. Final design (full line), $W_{TS} - 50$ μm (dashed line), and $W_{TS} + 50$ μm (dotted line).

that resonate in the 38 GHz band, as is illustrated in Fig. 6. If the slot width W_{TS} is decreased, the amount of coupling between QM_{TL} and QM_{TR} increases, and the resonances in the 38 GHz band diverge. When the slot width is increased, the coupling decreases and the resonances merge.

Fig. 7 depicts the simulated reflection coefficient for variations in the slot widths W_{MS1} and W_{MS2}. Decreasing both sloth widths results in increased coupling between the top and bottom cavities. As shown in Fig. 7, this results in an increased spacing between the resonances in the 28 GHz band and the resonances in the 38 GHz band. Alternatively, when W_{MS1} and W_{MS2} are increased, the distance between the pairs of resonances decreases.

All of the above validates the antenna operation principle as outlined in Section II-A. In the first step of the design, the dimensions of the QMSIW resonating cavities are determined as to obtain resonance frequencies that are in the frequency range of interest. In the following step, the dimensions of the slots between adjacent cavities are optimized and fine-tuned to obtain the desired antenna characteristics.

III. ANTENNA ARRAY PERFORMANCE

A compact four-element linear array configuration is constructed, as depicted in Fig. 8. A microstrip line corporate feeding network, consisting of two stages of power dividers, is exploited to excite the array elements. To facilitate
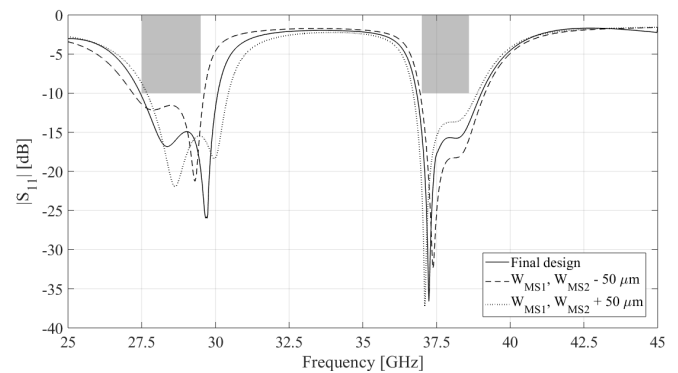

Fig. 7. Simulated reflection coefficient for variations on the slot widths W_{MS1} and W_{MS2}. Final design (full line), W_{MS1}, $W_{MS2} - 50$ μm (dashed line), and W_{MS1}, $W_{MS2} + 50$ μm (dotted line).
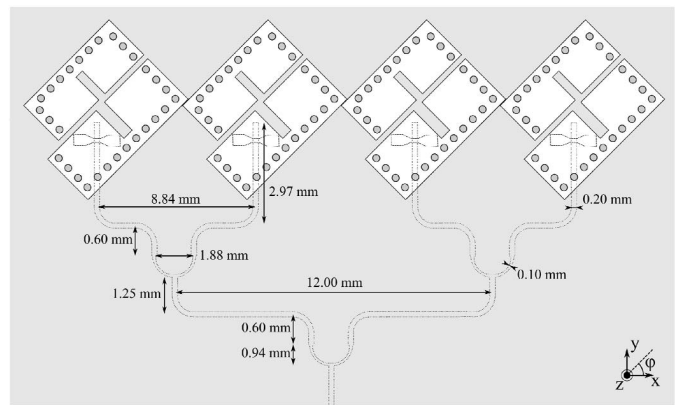

Fig. 8. Four-element linear array configuration with corporate microstrip line feeding network, consisting of two stages of power dividers. Dimensions of the array elements are shown in Fig. 1 and specified in Table I.

a straightforward implementation of the feeding structure, the elements in the array are rotated over an angle of 45°.

The simulated radiation patterns at 28 and 38 GHz, in both the E-plane ($\varphi = 90°$) and H-plane ($\varphi = 0°$), are depicted in Fig. 9. The simulations are performed on a model with a finite-ground plane with dimensions equal to 27.5×28.5 mm². At 28 and 38 GHz, a broadside array gain is achieved of, respectively, 10.1 and 10.2 dBi, while the directivity equals 11.88 and 11.94 dBi, respectively. In the 28 and 38 GHz band, the 3 dB beamwidth in the E-plane amounts to 21.6° and 18.6°, respectively. The sidelobe level remains below −8.5 and −13 dB in the 28 and 38 GHz band, respectively. Although a microstrip line feeding network, with aperture coupling, is implemented on the backplane of the array, front-to-back ratios of more than 8 and 18 dB are obtained in the lowest and highest band, respectively.

Clearly, parasitic radiation emanating from the feeding network is minimized by exploiting a bowtie slot and applying a limited substrate thickness of 100 μm for the feeding layer. Hence, a high antenna/platform isolation is obtained, facilitating straightforward integration with active electronics in the feeding layer, with a limited risk of unwanted and possibly harmful coupling.
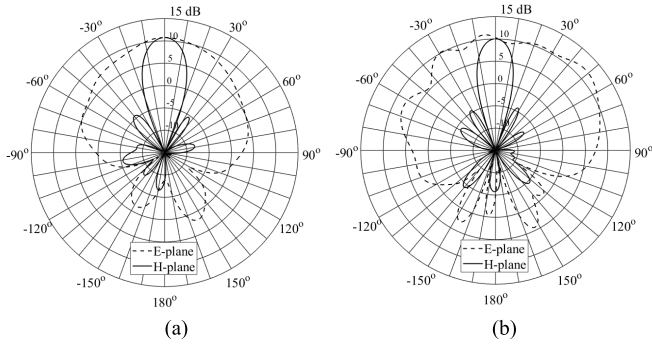
Fig. 9. Simulated radiation pattern of the four-element linear array at (a) 28 GHz and (b) 38 GHz in both the E-plane ($\varphi = 90°$) and H-plane ($\varphi = 0°$).

Fig. 11. Measured (solid line) reflection coefficient. Wideband behavior in both the 28 and 38 GHz band is obtained. Simulated results for the final design, with dimensions specified in Fig. 1 and Table I, (dotted line) and simulated results that include the quantified fabrication errors (dashed line) are shown as well.
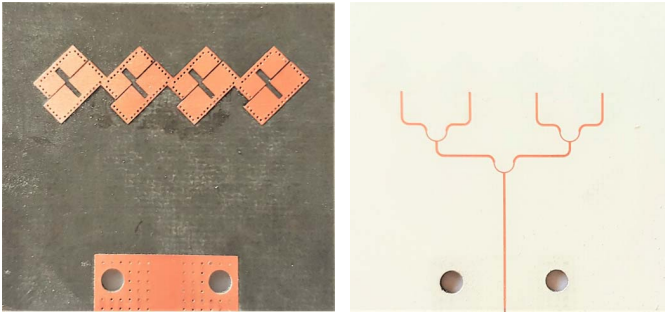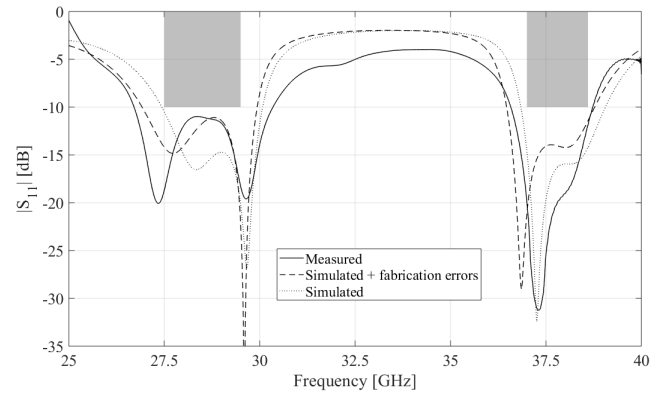

Fig. 10. Fabricated prototype of the (28,38) GHz dual-band coupled QMSIW 1 × 4 linear array. Antenna elements on Duroid 5880 top substrate layer (left) and corporate feeding network on RO4450F bottom substrate layer (right).

IV. FABRICATION PROCESS

The actual antenna array, of which each element consists of the four resonating cavities, is realized on a 508 μm Rogers Duroid 5880 laminate through standard PCB manufacturing. Next, further in-house processing is performed to realize the multilayer build-up, as depicted in Fig. 1. A 100 μm RO4450F bondply, serving as the substrate for the microstrip feeding network, and an 18 μm copper foil are sequentially laminated onto the backplane of the antenna structure. Finally, the microstrip feeding structure is realized through photolithography, arriving at the array prototype depicted in Fig. 10. Although, here, the RO4450F bondply is used for unconventional purposes, its electromagnetic and mechanical properties fit the application perfectly. First, it has a dielectric constant that is close to that of the top Duroid 5880 layer, enabling good coupling through the bowtie aperture. Second, this fabrication process allows for an asymmetric build-up of the multilayer PCB, which has clear benefits, i.e., the limited thickness of the bondply layer minimizes parasitic radiation from the microstrip feeding network, as was already demonstrated in Section III.

After fabrication, the prototypes are subjected to a thorough dimensional analysis to identify possible manufacturing errors. The most significant deviation from the simulation model is attributed to variations of the substrate thickness of the RO4450F layer for the feeding network. The targeted thickness of the feed layer is 100 μm, as specified in Fig. 1.

Nevertheless, the dimensional analysis reveals a substrate thickness of approximately 130 μm. This deviation has a nonnegligible effect on the mm-Wave characteristics of the dual-band antenna, as proven by the measured and simulated reflection coefficients in Fig. 11. If the measured $|S_{11}|$ (solid line) is compared to the simulated results of the final design (dotted line), with dimension as in Table I, a significant discrepancy is apparent. However, if the manufacturing errors are included in the simulation model (dashed line), the measured −10 dB impedance bandwidth agrees quite well with the simulation and covers both the proposed 5G frequency bands, as further specified in Section V. However, there are still minor discrepancies between the simulated and measured curves, which can possibly be attributed to the unconventional use of the RO4450F bondply and the experimental manufacturing techniques.

V. EXPERIMENTAL VALIDATION

The validation of the reflection coefficients of the fabricated prototypes is conducted using a Keysight N5247A PNA-X Microwave Network Analyzer and solder-free V-type (1.85 mm) End-Launch Connectors by Southwest Microwave [23]. The coaxial pin of the connectors is not soldered, but press fit onto the signal trace. To compensate for the additional capacitance generated by the interference fit, the signal trace is tapered and optimized to add inductance. A thru–reflect–line calibration kit [24] was designed and exploited to deembed the connector and feed line, as such positioning the port reference plane closer to the antenna. This allows for an adequate comparison between simulated and measured S-parameters.

The measured reflection coefficient, depicted in Fig. 11, reveals a −10 dB impedance bandwidth ranging from 26.71 to 30.36 GHz and from 36.59 to 38.78 GHz, resulting in a bandwidth of 3.65 and 2.19 GHz for the lower and higher frequency band, respectively. Clearly, the developed prototype entirely covers the 28 GHz (27.5–29.5 GHz) and 38 GHz band (37–38.6 GHz), making it an ideal candidate for 5G dual-band wireless systems.

Fig. 12. Measured versus simulated, including measurement connector, radiation pattern at 28 GHz, both in (a) E-plane ($\varphi = 0°$) and (b) H-plane ($\varphi = 90°$).

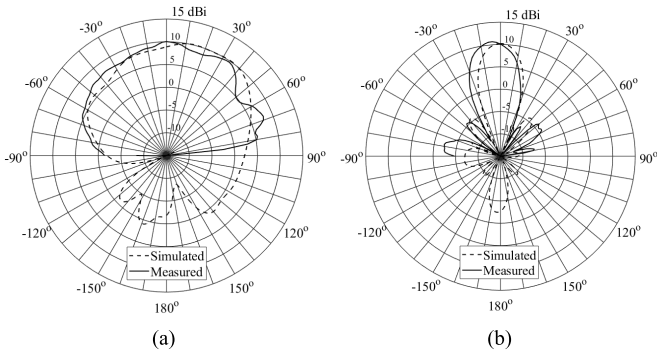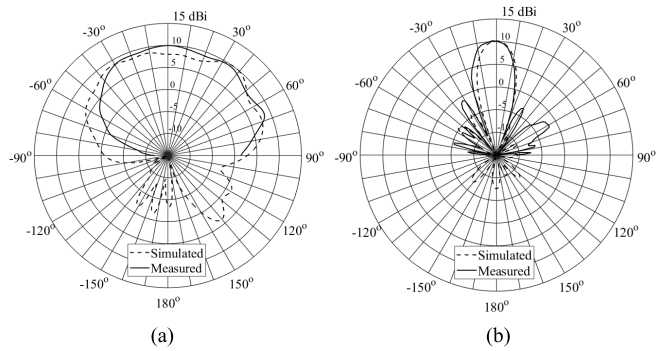

Fig. 13. Measured versus simulated, including measurement connector, radiation pattern at 38 GHz, both in (a) E-plane ($\varphi = 0°$) and (b) H-plane ($\varphi = 90°$).

The far-field performance of the antenna array is verified with an NSI-MI spherical near-field measurement range [25], inside an anechoic chamber with outer dimensions of $8 \times 4 \times 4$ m^3. Moreover, a model of the measurement connector is included in the simulations to enable an adequate comparison between measured and simulated radiation patterns.

The measured and simulated array gain patterns at 28 GHz, both in the E-plane ($\varphi = 0°$) and H-plane ($\varphi = 90°$), agree well, as demonstrated in Fig. 12. A broadside array gain of 10.06 dBi, a radiation efficiency of 75.75%, and a 3 dB H-plane beamwidth of approximately 25° are achieved. Similarly, the measured gain patterns at 38 GHz are depicted in Fig. 13. In this frequency band, the broadside array gain amounts to 10.2 dBi. Moreover, a radiation efficiency of 70.65% is achieved, and the 3 dB beamwidth in the H-plane equals approximately 20°. Owing to the 0.31 dB higher insertion loss in the corporate feeding network at 38 GHz, as compared to 28 GHz, the radiation efficiency is slightly lower in the highest frequency band. In addition, the far-field patterns have a slightly asymmetrical character, especially in the E-plane ($\varphi = 0°$). This is attributed to the presence of the bulky, solid metal measurement connector [23] in that plane.

As is clear from Figs. 12 and 13, there are still some minor discrepancies between the simulated and measured radiation patterns. More specifically, the main beam in the H-plane

at 28 GHz has slightly shifted, and the measured and simulated sidelobe levels at both frequencies do not agree perfectly. It needs to be noted that the slightest disturbance in the measurement environment affects the far-field pattern at these high-mm-Wave frequencies. The simulation model is made as exhaustive as possible, i.e., by including the measurement connector, to enable an adequate reproduction of the realistic measurement scenario. Nevertheless, there still is a certain amount of measurement overhead in terms of fixtures and cables that are unaccounted for in the model, causing minor discrepancies between measured and simulated results.

VI. CONCLUSION

A novel 1×4 (28,38) GHz dual-band antenna array topology, based on coupled QMSIW cavities, has been proposed, manufactured, and validated for operation in the 5G frequency bands at 28 and 38 GHz. Four miniaturized QMSIW resonant cavities are tightly coupled, causing mode bifurcation, and yielding an antenna topology with four distinct resonance frequencies. One pair of QMSIW cavities is tuned to resonate in the 28 GHz band, while the other pair is optimized for the 38 GHz band, accomplishing dual-band operation. Moreover, through skillful distribution of the pair of resonance peaks in both frequency ranges of interest, wideband operation is achieved in both bands. This innovative approach not only offers dual-band and wideband operation but, owing to the applied SIW miniaturization technique, yields an extremely compact array topology as well.

The array elements are realized on the top Duroid 5880 substrate layer, while the microstrip corporate feeding network is implemented on the thin bottom layer of RO4450F. Aperture coupling through an hourglass-shaped slot is exploited to excite the antenna array, as such maximizing the matching bandwidth. Moreover, due to the excellent shielding capabilities of the employed SIW technology and the aperture coupling feeding technique, a high antenna/platform isolation is achieved, facilitating straightforward integration with active electronics.

A measured -10 dB impedance bandwidth of 3.65 GHz (26.71–30.36 GHz) and 2.19 GHz (36.59–38.78 GHz) is achieved for the lowest and highest bands, respectively. As such, this novel topology covers both the 28 GHz (27.5–29.5 GHz) and 38 GHz (37–38.6 GHz) frequency bands, which are under strong consideration for future 5G applications. A measured broadside array gain of 10.06 dBi, a 3 dB beamwidth in the H-plane of approximately 25°, and a radiation efficiency of 75.75% are achieved at 28 GHz. At 38 GHz, the measured broadside gain amounts to 10.2 dBi, the radiation efficiency is 70.65%, and the 3 dB beamwidth in the H-plane is approximately 20°.

Taking all of the above into account, the proposed dual-band, high-gain, and narrow-beam antenna array topology is the ideal candidate for deployment in future 5G scenarios, e.g., as a base station antenna. The wideband performance in both frequency bands supports very high data rates, while the extremely compact dimensions facilitate easy and straightforward integration. Moreover, the dual-band operation benefits

the flexibility of the 5G wireless system, as it offers the possibility of switching the operational frequency under changing environmental conditions.

REFERENCES

[1] M. Bozzi, A. Georgiadis, and K. Wu, "Review of substrate-integrated waveguide circuits and antennas," *IET Microw. Antennas Propag.*, vol. 5, no. 8, pp. 909–920, Jun. 2011.

[2] K. K. Samanta, D. Stephens, and I. D. Robertson, "Design and performance of a 60-GHz multi-chip module receiver employing substrate integrated waveguides," *IET Microw., Antennas Propag.*, vol. 1, no. 5, pp. 961–967, Oct. 2007.

[3] K. Kuhlmann and A. F. Jacob, "Active 30 GHz antenna array for digital beamforming and polarization multiplexing," in *IEEE MTT-S Int. Microw. Symp. Dig.*, Anaheim, CA, USA, May 2010, pp. 1276–1279.

[4] F. Giuppi, A. Georgiadis, A. Collado, and M. Bozzi, "Active substrate integrated waveguide (SIW) antenna with phase-shifterless beam-scanning capabilities," in *IEEE MTT-S Int. Microw. Symp. Dig.*, Montreal, QC, Canada, Jun. 2012, pp. 1–3.

[5] H. Rogier *et al.*, "Novel wearable antenna systems for high datarate mobile communication in healthcare," in *Proc. 4th Int. Conf. Wireless Mobile Commun. Healthcare-Transf. Healthcare Through Innov. Mobile Wireless Technol. (MOBIHEALTH)*, Athens, Greece, 2014, pp. 188–191.

[6] F. Giuppi, A. Georgiadis, A. Collado, M. Bozzi, and L. Perregrini, "Tunable SIW cavity backed active antenna oscillator," *Electron. Lett.*, vol. 46, no. 15, pp. 1053–1055, Jul. 2010.

[7] C. Jin, R. Li, A. Alphones, and X. Bao, "Quarter-mode substrate integrated waveguide and its application to antennas design," *IEEE Trans. Antennas Propag.*, vol. 61, no. 6, pp. 2921–2928, Jun. 2013.

[8] Q. Wu, H. Wang, C. Yu, and W. Hong, "Low-profile circularly polarized cavity-backed antennas using SIW techniques," *IEEE Trans. Antennas Propag.*, vol. 64, no. 7, pp. 2832–2839, Jul. 2016.

[9] T. Deckmyn *et al.*, "A novel 60 GHz wideband coupled half-mode/quarter-mode substrate integrated waveguide antenna," *IEEE Trans. Antennas Propag.*, vol. 65, no. 12, pp. 6915–6926, Dec. 2017.

[10] N. Ashraf, O. Haraz, M. A. Ashraf, and S. Alshebeili, "28/38-GHz dual-band millimeter wave SIW array antenna with EBG structures for 5G applications," in *Proc. Int. Conf. Inf. Commun. Technol. Res. (ICTRC)*, Abu Dhabi, United Arab Emirates, 2015, pp. 5–8.

[11] T. Zhang, W. Hong, Y. Zhang, and K. Wu, "Design and analysis of SIW cavity backed dual-band antennas with a dual-mode triangular-ring slot," *IEEE Trans. Antennas Propag.*, vol. 62, no. 10, pp. 5007–5016, Oct. 2014.

[12] M.-J. Chiang, S. Wang, and C.-C. Hsu, "Miniaturised printed slot antenna with multi-ring technique for dual-band and broadband operations," *IET Microw., Antennas Propag.*, vol. 8, no. 6, pp. 409–414, Apr. 2014.

[13] T.-Y. Lin, T. Chiu, and D.-C. Chang, "Design of dual-band millimeter-wave Antenna-in-Package using flip-chip assembly," *IEEE Trans. Compon., Packag., Manuf. Technol.*, vol. 4, no. 3, pp. 385–391, Mar. 2014.

[14] P. Burasa, T. Djerafi, N. G. Constantin, and K. Wu, "On-chip dual-band rectangular slot antenna for single-chip millimeter-wave identification tag in standard CMOS technology," *IEEE Trans. Antennas Propag.*, vol. 65, no. 8, pp. 3858–3868, Aug. 2017.

[15] M. Mujumdar and A. Alphones, "Eighth mode substrate integrated waveguide dual band resonator antennas," *IET Microw., Antennas Propag.*, vol. 11, no. 9, pp. 1262–1266, 2017.

[16] Q. Wu, J. Yin, C. Yu, H. Wang, and W. Hong, "Low-profile millimeter-wave SIW cavity-backed dual-band circularly polarized antenna," *IEEE Trans. Antennas Propag.*, vol. 65, no. 12, pp. 7310–7315, Dec. 2017.

[17] H. Lee, Y. Sung, C. T. M. Wu, and T. Itoh, "Dual-band and polarization-flexible cavity antenna based on substrate integrated waveguide," *IEEE Antennas Wireless Propag. Lett.*, vol. 15, pp. 488–491, 2016.

[18] S. Agneessens and H. Rogier, "Compact half diamond dual-band textile HMSIW on-body antenna," *IEEE Trans. Antennas Propag.*, vol. 62, no. 5, pp. 2374–2381, May 2014.

[19] W. Li, K. Da Xu, X. Tang, Y. Yang, Y. Liu, and Q. H. Liu, "Substrate integrated waveguide cavity-backed slot array antenna using high-order radiation modes for dual-band applications in *K*-band," *IEEE Trans. Antennas Propag.*, vol. 65, no. 9, pp. 4556–4565, Sep. 2017.

[20] D.-F. Guan, Z.-P. Qian, W.-Q. Cao, L.-Y. Ji, and Y.-S. Zhang, "Compact SIW annular ring slot antenna with multiband multimode characteristics," *IEEE Trans. Antennas Propag.*, vol. 63, no. 12, pp. 5918–5922, Dec. 2015.

[21] S. Mukherjee and A. Biswas, "Design of dual band and dual-polarised dual band SIW cavity backed bow-tie slot antennas," *IET Microw., Antennas Propag.*, vol. 10, no. 9, pp. 1002–1009, 2016.

[22] J.-S. Hong and M. J. Lancaster, "Couplings of microstrip square open-loop resonators for cross-coupled planar microwave filters," *IEEE Trans. Microw. Theory Techn.*, vol. 44, no. 11, pp. 2099–2109, Nov. 1996.

[23] Southwest Microwave. (2016). *1.85 mm (V) DC to 67.0 GHz Connectors.* [Online]. Available: http://mpd.southwestmicrowave.com

[24] G. F. Engen and C. A. Hoer, "Thru-reflect-line: An improved technique for calibrating the dual six-port automatic network analyzer," *IEEE Trans. Microw. Theory Techn.*, vol. MTT-27, no. 12, pp. 987–993, Dec. 1979.

[25] NSI-MI Technologies. (2017). *Spherical Near-Field Scanner Systems.* [Online]. Available: https://www.nsi-mi.com
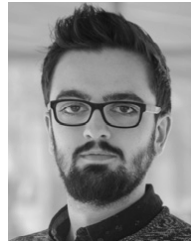
Thomas Deckmyn (S'17) was born in 1993. He received the M.Sc. degree in electrical engineering from Ghent University, Ghent, Belgium, in 2015.

From 2015 to 2017, he was involved in the Horizon 2020 Flex5Gware Project, where he co-developed an integrated millimeter-wave (mm-Wave) active antenna array for future 5G devices. He is currently a Ph.D. Researcher with the Department of Information Technology, IDLab Electromagnetics Group, Ghent University/imec. His current research interests include the design and implementation of mm-Wave antenna solutions for next-generation wireless systems.

Maarten Cauwe (M'10) received the M.Sc. degree in electronics engineering from Ghent University, Ghent, Belgium, and the Ph.D. degree from the Center for Microsystems Technology (CMST), Ghent University/imec.

He is currently leading the Advanced Packaging Team, CMST, where he is involved in several projects concerning substrate technologies, chip assembly, medical packaging, and chip embedding. His past research was focused on component embedding in printed circuit boards, where he was involved from the first exploratory projects (Hiding Dies, from 2004 to 2006) until the commercial industrialization of this technology in the frame of the HERMES project from 2008 to 2011. He recently coordinated a project on this topic in cooperation with the European Space Agency from 2014 to 2016. Other activities involve implantable packaging and flexible electronics.

Dries Vande Ginste (SM'12) received the M.S. and Ph.D. degrees in electrical engineering from Ghent University, Ghent, Belgium, in 2000 and 2005, respectively.

In 2004, he joined the Department of Electrical and Computer Engineering, University of Illinois at Urbana–Champaign, IL, USA, as a Visiting Scientist. In 2011, he joined the EMC Group, Dipartimento di Elettronica, Politecnico di Turin, Turin, Italy, as a Visiting Professor. He is currently an Associate Professor with the Department of Information Technology, Ghent University, and a Guest Professor with imec. He has authored or co-authored over 150 papers in international journals and conference proceedings. His current research interests include computational electromagnetics, electromagnetic compatibility, signal and power integrity, and antenna design.

Dr. Vande Ginste was a recipient of the International Union of Radio Science (URSI) Young Scientist Award at the 2011 URSI General Assembly and Scientific Symposium, the Best Poster Paper Award at the 2012 IEEE Electrical Design of Advanced Packaging and Systems Symposium (EDAPS), the Best Paper Award at the 2013 IEEE Workshop on Signal and Power Integrity, the Best Paper Award at the 2013 IEEE International Conference on Electrical Performance of Electronic Packaging and Systems, and the Best Paper Award at the 2016 IEEE EDAPS. He served as the Chair for the 2014 IEEE Workshop on Signal and Power Integrity.

Hendrik Rogier (SM'06) received the M.Sc. and Ph.D. degrees in electrical engineering from Ghent University, Ghent, Belgium, in 1994 and 1999, respectively.

From 2003 to 2004, he was a Visiting Scientist with the Mobile Communications Group, Vienna University of Technology, Vienna, Austria. He is a currently a Full Professor with the Department of Information Technology, Ghent University, a Guest Professor with imec, Ghent, and a Visiting Professor with the University of Buckingham, Buckingham, U.K. He has authored or co-authored over 155 papers in international journals and 176 contributions in conference proceedings. His current research interests include antenna systems, radio wave propagation, body-centric communication, numerical electromagnetics, electromagnetic compatibility, and power/signal integrity.

Dr. Rogier was a recipient of the International Union of Radio Science (URSI) Young Scientist Award, twice, at the 2001 URSI Symposium on Electromagnetic Theory and at the 2002 URSI General Assembly, the 2014 Premium Award for Best Paper in *IET Electronics Letters*, the Best Paper Award First Place at the 2016 IEEE MTT-S Topical Conference on Wireless Sensors and Sensor Networks, the Best Poster Paper Award at the 2012 IEEE Electrical Design of Advanced Packaging and Systems Symposium, the Best Paper Award at the 2013 IEEE Workshop on Signal and Power Integrity, and the Joseph Morrissey Memorial Award for the First Best Scientific Paper at the 2013 Joint Meeting of the Bioelectromagnetics Society and the European Bioelectromagnetics Association. He is an Associate Editor of *IET Electronics Letters*, *IET Microwaves, Antennas and Propagation*, and the IEEE TRANSACTIONS ON MICROWAVE THEORY AND TECHNIQUES. He acts as the URSI Commission B Representative for Belgium. Within the IEEE Microwave Theory and Techniques Society, he is a member of the Technical Committee 24 on RFID technology, and within the European Microwave Association, he is a member of the Governing Board of Topical Group MAGEO on Microwaves in Agriculture, Environment, and Earth Observation.

Sam Agneessens (S'14–M'16) received the M.S. and Ph.D. degrees in electrical engineering from Ghent University, Ghent, Belgium, in 2011 and 2015.

He is currently an Assistant Professor with Ghent University and a Post-Doctoral Fellow with Research Foundation—Flanders, Brussel, Belgium, with the Department of Information Technology, IDLab Electromagnetic Group, Ghent, and the Centre for Microsystems, Ghent University/imec. His current research interests include millimeter-wave antenna-on-package and active antenna solutions for 5G systems, as well as robust antenna systems for wearable applications relying on unconventional substrates.

Dr. Agneessens was a recipient of the International Union of Radio Science (URSI) Young Scientist Award at the 2014 URSI General Assembly, the 2014 Premium Award for Best Paper in *IET Electronics Letters*, and the Honorable Mention in the Student Paper Competition at the 2014 IEEE International Symposium on Antennas and Propagation and USNC–URSI Radio Science Meeting.